AMERICAN SOCIETY FOR MICROBIOLOGY | Infection and Immunity®

MOLECULAR PATHOGENESIS

Tissue Tropism in Streptococcal Infection: Wild-Type M1T1 Group A *Streptococcus* Is Efficiently Cleared by Neutrophils Using an NADPH Oxidase-Dependent Mechanism in the Lung but Not in the Skin

Benfang Lei,[a] Dylan Minor,[a] Wenchao Feng,[a] Maria Jerome,[a] Mark T. Quinn,[a] Mark A. Jutila,[a] Mengyao Liu[a]

[a]Department of Microbiology and Immunology, Montana State University, Bozeman, Montana, USA

ABSTRACT Group A *Streptococcus* (GAS) commonly causes pharyngitis and skin infections. Little is known why streptococcal pharyngitis usually does not lead to pneumonia and why the skin is a favorite niche for GAS. To partially address these questions, the effectiveness of neutrophils in clearing wild-type (wt) M1T1 GAS strain MGAS2221 from the lung and from the skin was examined in murine models of intratracheal pneumonia and subcutaneous infection. Ninety-nine point seven percent of the MGAS2221 inoculum was cleared from the lungs of C57BL/6J mice at 24 h after inoculation, while there was no MGAS2221 clearance from skin infection sites. The bronchial termini had robust neutrophil infiltration, and depletion of neutrophils abolished MGAS2221 clearance from the lung. Phagocyte NADPH oxidase but not myeloperoxidase was required for MGAS2221 clearance. Thus, wt M1T1 GAS can be cleared by neutrophils using an NADPH oxidase-dependent mechanism in the lung. MGAS2221 induced robust neutrophil infiltration at the edge of skin infection sites and throughout infection sites at 24 h and 48 h after inoculation, respectively. Neutrophils within MGAS2221 infection sites had no nuclear staining. Skin infection sites of streptolysin S-deficient MGAS2221 Δ*sagA* were full of neutrophils with nuclear staining, whereas MGAS2221 Δ*sagA* infection was not cleared. Gp91^{phox} knockout (KO) and control mice had similar GAS numbers at skin infection sites and similar abilities to select SpeB activity-negative (SpeB^{A-}) variants. These results indicate that phagocyte NADPH oxidase-mediated GAS killing is compromised in the skin. Our findings support a model for GAS skin tropism in which GAS generates an anoxic niche to evade phagocyte NADPH oxidase-mediated clearance.

KEYWORDS clearance, NADPH oxidase, group A streptococcus, myeloperoxidase, neutrophil, streptolysin S, tissue tropism

Group A *Streptococcus* (GAS) is a major human pathogen that commonly causes pharyngitis and skin infections. It is estimated that there are 616 million cases of strep throat and 111 million incidences of GAS skin infections each year globally (1). GAS also occasionally causes severe invasive infections, such as necrotizing fasciitis, pneumonia, and sepsis. There are about 10,000 cases of severe invasive GAS infections each year in the United States that are most frequently associated with GAS of the M protein serotypes M1, M12, M28, M89, and M3 (2). The currently circulating M1 GAS type belongs to the pandemic M1T1 clone. The M1T1 clone has evolved by the acquisition of DNase Sda1- and superantigen SpeA-encoding prophages and the replacement of a 36-kb chromosomal region of pre-1980 M1 GAS with that of *emm*12 GAS, which contains the NAD^+ nucleosidase (NADase) and streptolysin O genes (3–5). It is believed that M1T1 GAS is currently the most prevalent GAS pathogen in pharyngeal, skin, and invasive infections (2, 6, 7).

Citation Lei B, Minor D, Feng W, Jerome M, Quinn MT, Jutila MA, Liu M. 2019. Tissue tropism in streptococcal infection: wild-type M1T1 group A *Streptococcus* is efficiently cleared by neutrophils using an NADPH oxidase-dependent mechanism in the lung but not in the skin. Infect Immun 87:e00527-19. https://doi.org/10.1128/IAI.00527-19.

Editor Nancy E. Freitag, University of Illinois at Chicago

Address correspondence to Benfang Lei, blei@montana.edu.

Received 9 July 2019
Accepted 14 July 2019
Accepted manuscript posted online 22 July 2019
Published 19 September 2019

Invasive GAS isolates frequently carry CovRS and RopB mutations that are associated with hypervirulence of invasive GAS isolates (8, 9). CovRS (also known as CsrRS) is the two-component regulatory system that negatively regulates multiple virulence factors (10–13), and RopB is the transcription activator of the protease SpeB (14). GAS CovRS and RopB mutants can cause pulmonary infection in an intratracheal murine pneumonia model (15). However, CovRS and RopB mutants appear to be selected during infection and are unable to transmit, and the majority of clinical isolates have wild-type (wt) CovRS and RopB (16). Strep throat is highly contagious but usually does not develop into pneumonia. Little is known about why GAS infections of the upper respiratory tract usually do not lead to lower respiratory tract infections.

GAS isolates were first serologically typed based on the M protein and T antigen (17). Genotyping based on the sequence of the M protein gene, *emm*, has been more widely used to conveniently classify GAS isolates (18). Expanded genotyping has found three *emm* pattern groups that display different tissue tropisms of infection at the skin versus at the throat (19). However, little is known about why the skin is one of the favorite niches for GAS.

GAS produces an abundance of extracellular virulence factors to mediate its pathogenesis (20, 21). These virulence factors include the M protein (22), C5a peptidase ScpA (23), the hyaluronic acid capsule synthesized by HasABC (24), CXC chemokine peptidase SpyCEP (25), platelet-activating factor (PAF) acetylhydrolase Sse (26), streptolysin O (Slo) (27), NADase Nga (28), opsonophagocytosis-inhibiting protein Mac (29), and streptolysin S (SLS). SLS is a potent cytolytic toxin that confers the beta-hemolytic activity of GAS, and this toxin is a nonimmunogenic peptide modified from the prepropeptide that is encoded by the *sagA* gene (30). Most of these virulence factors are involved in evasion of neutrophil responses, which supports the finding that neutrophil responses have a critical role in the fight against GAS infections.

We are interested in two questions on GAS tissue tropism: why do upper respiratory tract GAS infections not lead to lower respiratory tract infections, and why is the skin a favorite niche for GAS? We hypothesize that neutrophils can effectively clear GAS with functional CovRS and RopB or wt GAS from the lung but not from the skin. We tested this hypothesis by examining the neutrophil-mediated clearance of wt M1T1 strain MGAS2221 from lung and skin infections of mice. We found that wt M1T1 GAS can be cleared from the lung by neutrophils with an NADPH oxidase-dependent mechanism but that phagocyte NADPH oxidase-mediated GAS killing is compromised in the skin. The findings support a model for GAS skin tropism in which GAS generates an anoxic environment in the skin to evade phagocyte NADPH oxidase-mediated clearance.

RESULTS

Wild-type M1T1 GAS is effectively cleared from the lung but not from the skin. To understand the basis for the GAS tropism for the skin but not for the lung, MGAS2221, a representative strain of the M1T1 GAS subclone with functional or wild-type covRS and ropB genes, was used to compare bacterial clearances from lung and skin infections of mice. The lung and skin infections were induced by intratracheal and subcutaneous inoculations, respectively. In comparison with the number of viable GAS bacteria at 1 h after inoculation, 99.7% of GAS bacteria in the lung were cleared at 24 h after intratracheal inoculation ($P = 0.0007$); however, the numbers of viable GAS bacteria at skin infection sites were similar at 1 h and 24 h after subcutaneous inoculation ($P = 0.84$) (Fig. 1A). As shown in a Gram stain of lung tissue at 30 min after intratracheal MGAS2221 inoculation (Fig. 1B), GAS bacteria stained as blue spots and scattered at bronchial termini and along the alveolar ducts. There were no significant numbers of inflammatory cells at 30 min after inoculation. At 24 h after inoculation, clusters of inflammatory cells were found at the bronchial termini and along the alveolar ducts as shown in the hematoxylin and eosin (H&E) staining analysis of the lung sections (Fig. 1C), in which hematoxylin stains the nuclei of inflammatory cells blue and in which eosin stains their cytoplasm pink. The Gram stain analysis of lung sections at 24 h after MGAS2221 inoculation did not reveal any blue GAS spots, confirming the

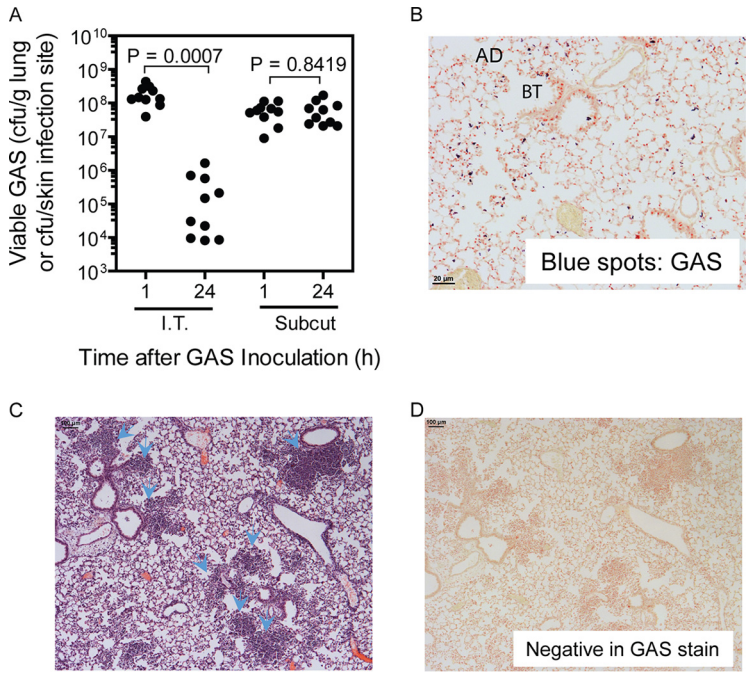

FIG 1 MGAS2221 is effectively cleared from pulmonary infections but not from subcutaneous infections of C57BL/6J mice. In total, 1.2×10^8 and 0.8×10^8 CFU of MGAS2221 were inoculated into mice intratracheally (I.T.) and subcutaneously (Subcut), respectively. (A) GAS loads in the lung or in skin infection sites at 1 h and 24 h after inoculation. (B and D) Representative Gram stain images of lung sections at 30 min (×20 magnification) (B) and 24 h (×4 magnification) (D) after inoculation. AD and BT, alveolar duct and bronchial terminus, respectively. Panel B shows GAS bacteria as blue spots at bronchial termini and along alveolar ducts, while panel D shows the absence of stained GAS bacteria. (C) Representative H&E-stained image of a lung section at 24 h after inoculation. The arrowheads indicate the clumps of recruited neutrophils at the bronchial termini or along alveolar ducts.

efficient clearance of GAS from lung infections (Fig. 1D). Thus, MGAS2221 induced robust inflammatory cell infiltration and was efficiently cleared from the lungs of mice. In contrast, MGAS2221 was not cleared from subcutaneous infection sites in mice.

Wild-type M1T1 GAS is cleared from the lung by neutrophils. To determine whether neutrophils play a critical role in the MGAS2221 clearance from the lung, neutrophils were depleted through treatment with anti-Ly6G monoclonal antibody RB6-8C5 (31, 32), and the effect of the neutrophil depletion on GAS clearance from the lung was examined. Bronchoalveolar lavage fluids (BALF) were collected from the neutropenic and control mice at 24 h after intratracheal MGAS2221 inoculation. Two aliquots of each BALF sample were used in cytospin analysis for differential cell counting of neutrophils and macrophages. In this analysis, inflammatory cells and bacteria in one aliquot of each BALF sample were deposited on a cytospin slide using a cytospin centrifuge and stained for calculating the percentages of neutrophils and macrophages among inflammatory cells, and another BALF aliquot was used to determine the total number of viable cells by trypan blue exclusion counting. A third BALF aliquot was used to quantify GAS bacteria by plating. BALF samples from control mice that were treated with control antibody LTF-2 had numerous neutrophils and few bacteria (Fig. 2A), whereas BALF from RB6-8C5-treated mice contained fewer neutrophils and numerous free bacteria (Fig. 2B). Differential cell counting in the cytospin analysis found that BALF from control mice contained $(2.7 \pm 1.8) \times 10^6$ neutrophils and $(1.5 \pm 0.5) \times 10^5$ macrophages, while BALF from mice treated with RB6-8C5 had $(6.8 \pm 2.6) \times 10^4$ neutrophils and $(1.6 \pm 0.9) \times 10^5$ macrophages, representing a 97% reduction of egressed neutrophils but no significant change in numbers of macrophages in the RB6-8C5-treated mice in comparison with that in control mice (Fig. 2C). The numbers of viable GAS bacteria in the BALF samples from RB6-8C5-treated mice

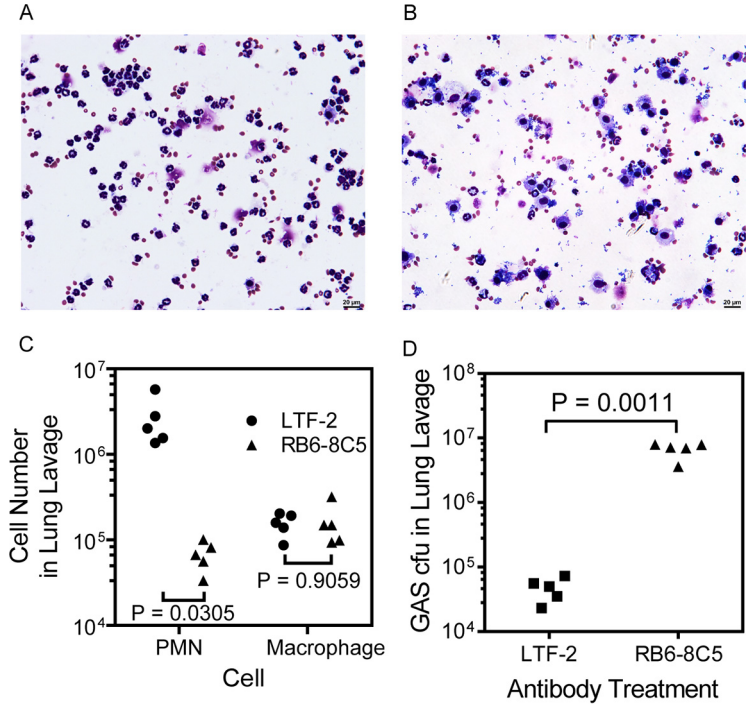

FIG 2 Depletion of neutrophils by anti-Ly6G antibody abolishes MGAS2221 clearance from the lung. RB6-8C5 MAb and control antibody LTF-2 were injected intraperitoneally into C57BL/6J mice, and 24 h later, 2.8×10^7 CFU of MGAS2221 was inoculated into the trachea. (A and B) Representative images of cytospin slides of BALF from control (A) and RB6-8C5-treated (B) mice. (C) Numbers of neutrophils and macrophages in 1 ml BALF collected at 24 h after GAS inoculation, as determined by cytospin analysis. PMN, polymorphonuclear macrophages. (D) Numbers of GAS bacteria in BALF from RB6-8C5-treated and control mice. Statistical analysis for *P* values was carried out with the unpaired *t* test with Welch's correction.

were 140-fold higher than those from control mice (Fig. 2D). Thus, RB6-8C5 treatment reduced neutrophil infiltration and compromised GAS clearance from the pulmonary infection.

RB6-8C5 can deplete both neutrophils and a subset of inflammatory monocytes that turn into recruited macrophages at infection sites (31). However, RB6-8C5 treatment did not alter the numbers of macrophages in the BALF samples, suggesting that lungs with MGAS2221 infection do not have significant numbers of recruited macrophages by 24 h after inoculation or that the RB6-8C5 treatment did not affect the numbers of macrophages recruited. To determine whether the inflammatory cells at the bronchial termini in Fig. 1C were primarily neutrophils, sections of the lung samples were examined by immunohistochemical staining using anti-F4/80 and anti-MPO antibodies. F4/80, an epidermal growth factor (EGF)-like module-containing mucin-like hormone receptor-like 1, is a macrophage marker. Myeloperoxidase (MPO) is a major constituent of the azurophilic cytoplasmic granules (33). A few F4/80-positive cells or macrophages (Fig. 3A) but numerous MPO-positive cells or neutrophils (Fig. 3B) were detected at the bronchial termini of the lung sections. These results indicate that inflammatory cells at the bronchial termini were mainly neutrophils up to 24 h after GAS inoculation. To further illustrate whether macrophages are important for GAS clearance in lung infections, the stained cytospin samples on slides for Fig. 2A and B were examined at $\times 40$ magnification. A majority of the macrophages in the BALF samples from RB6-8C5-treated mice did not take up MGAS2221, even when numerous GAS bacteria were present (Fig. 3C). For the BALF samples from control mice, a small portion of neutrophils in BALF from infected control mice had associated GAS (Fig. 3D), which was apparently due to efficient clearance. These results indicate that neutrophils play a dominant role in the killing of MGAS2221 during lung infection.

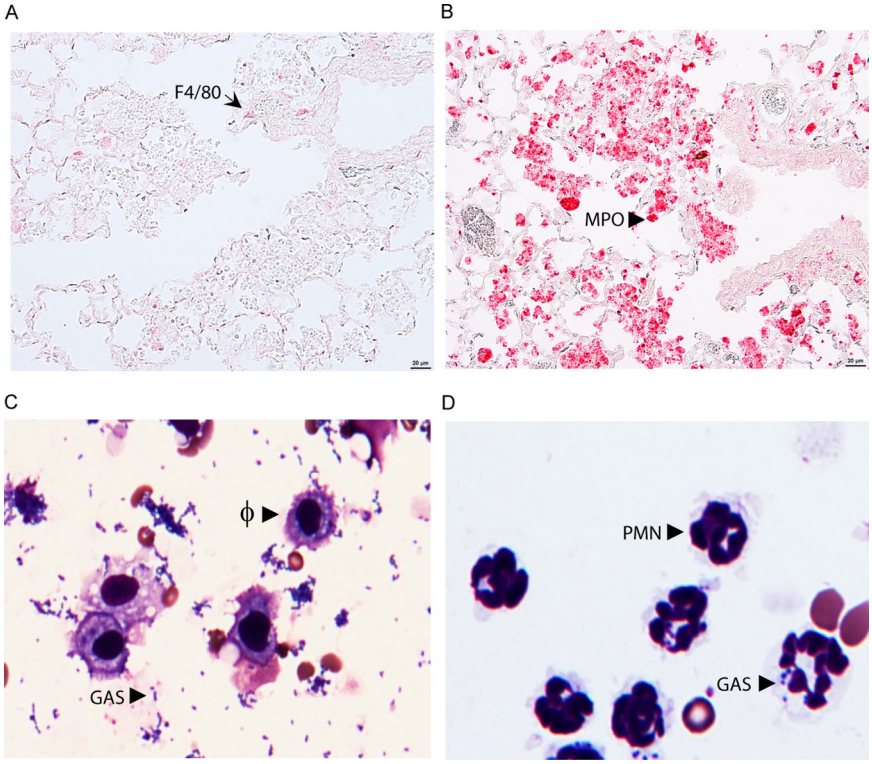

FIG 3 Supporting evidence for MGAS2221 clearance by neutrophils in the lung. (A and B) Images of anti-F4/80 and anti-myeloperoxidase (MPO) immunohistochemistry staining of lung sections showing a few F4/80-positive macrophages (A) and numerous MPO-positive neutrophils (B) at the bronchial termini at 24 h after intratracheal MGAS2221 inoculation for the pulmonary infection samples in Fig. 1. The immunostaining had no hematoxylin counterstain. (C and D) Images of cytospin slides of BALF from experiments whose results appear in Fig. 2. (C) Numerous free GAS bacteria and the inability of resident macrophages (Φ) to phagocytose GAS in RB6-8C5-treated mice; (D) no free bacteria and GAS association with a small portion of neutrophils (PMN) in control mice.

NADPH oxidase is critical for the clearance of MGAS2221 from the lung. The NADPH oxidase in the membranes of neutrophil phagosomes catalyzes electron transfer from NADPH to oxygen, generating superoxide, which is subsequently converted into a range of other reactive oxygen species (34). Gp91^{phox} is the beta chain of the catalytic subunit of the NADPH oxidase and encoded by the X-linked CYBB gene. The oxidative burst from the NADPH oxidase reaction is essential for the killing of a number of microorganisms. To determine whether NADPH oxidase-mediated killing plays a critical role in the clearance of MGAS2221 from the lung by neutrophils, we examined whether MGAS2221 is cleared from gp91^{phox} knockout (KO) mice (female gp91$^{phox-/-}$ and male gp91^{phox-} mice) (35). At 24 h after intratracheal MGAS2221 inoculation, the means ± standard deviations of the GAS loads in the lungs of gp91^{phox} KO mice were (5.2 ± 3.7) × 10^8 CFU/g tissue, which was 1,000-fold higher than that in the lungs of C57BL/6J mice [(5.1 ± 6.0) × 10^5 CFU/g] (Fig. 4A). These data represent a 6-fold increase in GAS numbers in gp91^{phox} KO mice and a 171-fold decrease in GAS numbers in C57BL/6J mice compared to numbers in the inoculum. In contrast, there was no significant difference between the numbers of viable MGAS2221 bacteria at skin infection sites between C57BL/6J and gp91^{phox} KO mice (Fig. 4A). Unlike in Fig. 1D, where lung sections of infected C57BL/6J mice were negative by GAS staining, lung sections of infected gp91^{phox} KO mice at 24 h after intratracheal GAS inoculation were positive for GAS in Gram stains (Fig. 4B). There were numerous GAS-positive clumps in Gram-stained slides like the one circled in Fig. 4B. There were many neutrophils like the one indicated with the arrow in Fig. 4C, which exhibited nuclear staining in H&E stains of the same lung infection samples. However, as with the one circled in Fig. 4B, the

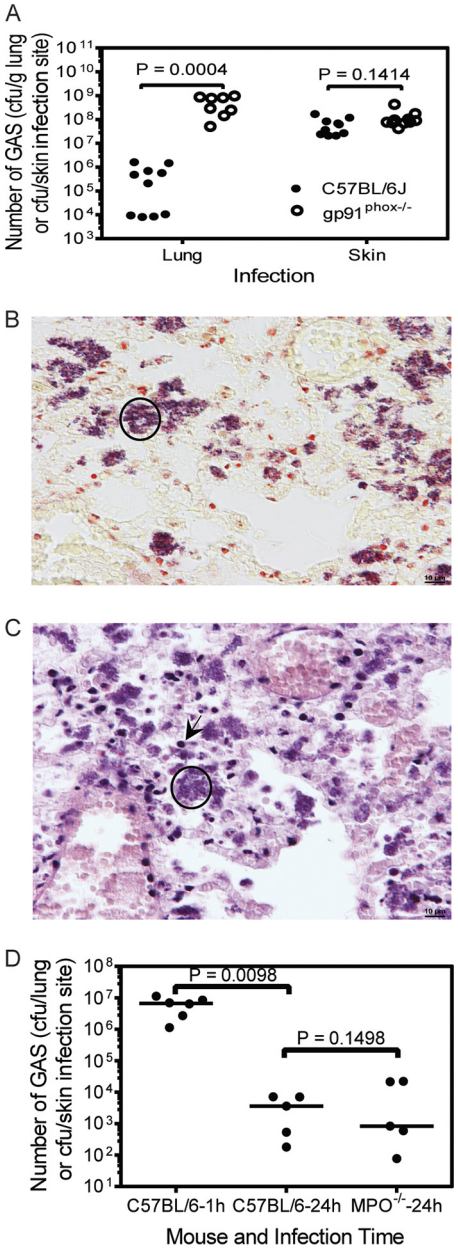

FIG 4 MGAS2221 clearance from the lung requires NADPH oxidase but is independent of myeloperoxidase. (A to C) MGAS2221 was not cleared from the lungs of gp91$^{phox-/-}$ mice. C57BL/6J or gp91$^{phox-/-}$ mice were inoculated intratracheally and subcutaneously with 1.1×10^8 CFU and 5.9×10^7 CFU of MGAS2221, respectively, and euthanized at 24 h after inoculation. (A) Numbers of GAS CFU in the lung or at the skin infection sites of C57BL/6J and gp91$^{phox-/-}$ mice at 24 h after inoculation. (B and C) Representative images of Gram (B) and H&E (C) staining of lung sections of gp91$^{phox-/-}$ mice with pulmonary infection. The circle in panel B indicates one of many GAS clumps. The circle in panel C shows the lack of nuclear staining with hematoxylin of the location with the GAS clumps, and the arrow shows neutrophils with nuclear staining with hematoxylin in H&E stains. Figure 1C and D can be used as a comparison for panels C and B, respectively, for the effect of the gp91 knockout on the histopathology of MGAS2221 lung infection. (D) MGAS2221 clearance is independent of myeloperoxidase. C57BL/6J or MPO$^{-/-}$ mice were inoculated intratracheally with 8.7×10^6 CFU of MGAS2221. Presented are the numbers of GAS CFU in the lungs at 1 or 24 h after inoculation. Statistical analysis for *P* values was performed with the unpaired *t* test with Welch's correction.

location of the GAS clumps in Fig. 4C did not exhibit nuclear staining with H&E stain. GAS bacteria in the lungs of gp91^{phox} KO mice were associated mainly with necrotic debris of inflammatory cells. These results indicate that the neutrophil NADPH oxidase is required for GAS clearance in the murine pneumonia infection model. One mecha-

nism of NADPH oxidase-mediated bacterial killing is MPO-catalyzed oxidation of chloride, which generates toxic hypochlorous acid (35). To determine whether NADPH oxidase-mediated GAS clearance from the lung depends on myeloperoxidase, MGAS2221 clearances from C57BL/6J and MPO KO (36) mice were compared. GAS loads in the lungs of $MPO^{-/-}$ and C57BL/6J mice at 24 h after intratracheal inoculation were similar ($P = 0.1489$) and were >1,500-fold lower that those at 1 h after inoculation (Fig. 4D). Thus, myeloperoxidase is not essential for NADPH oxidase-mediated GAS clearance from the lung.

Inability of neutrophils to clear MGAS2221 at subcutaneous infection sites. To understand why MGAS2221 was not efficiently cleared from the skin, we analyzed the MGAS2221 infection sites on days 1, 2, and 4 after subcutaneous inoculation by immunohistochemistry (IHC) staining using anti-MPO antibodies and hematoxylin counterstain. We intended to determine whether there was inhibition of neutrophil infiltration inside infection sites and/or cytotoxic killing of recruited neutrophils to avoid GAS killing. The IHC staining method that we used stained MPO red, and hematoxylin stained the nuclei of host cells blue. GAS can cause necrosis of neutrophils to avoid killing (37). Necrosis of cells leads to the loss of nuclei, resulting in uniform eosin staining without nuclear staining with hematoxylin in H&E stain (38). Thus, necrotic neutrophils should have red MPO staining but do not have nuclear staining with hematoxylin. MPO staining inside MGAS2221 infection sites at 24 h after inoculation was not intense (Fig. 5A), indicating that neutrophil recruitment was not robust up to 24 h after inoculation. Intense MPO staining was present inside infection sites on day 2 (Fig. 5C) and day 4 (Fig. 5E) after inoculation. A layer of neutrophils at the edges of infection sites exhibited nuclear staining with hematoxylin, which is indicated by the braces in Fig. 5A, C, and E. In contrast, the majority of cells inside infection sites that were positive for MPO staining had no nuclear staining with hematoxylin. These results indicate that recruited neutrophils inside infection sites had gone through necrosis and lost the nucleus. To estimate the relative levels of neutrophils at skin infection sites, the ImageJ software (https://imagej.nih.gov/ij/) was used to measure the relative average intensities of MPO staining of uninfected skin or at infection sites for the blue channel of the MPO IHC images (5 mice per group). The blue-channel images were used to reduce the interference of the hematoxylin staining of some neutrophils. The red staining of MPO leads to the absorbance of blue light. Thus, the relative blue-channel intensities of MPO staining (the intensity of uninfected skin minus the intensity of infection sites) represent the relative levels of recruited neutrophils at infection sites. Fig. 5B shows the ImageJ analysis data and displays the average MPO staining values of 37.6, 73.3, and 91.5 for infection sites at days 1, 2, and 4, respectively. From these staining data, the levels of recruited neutrophils at infection sites on day 1 and day 2 were estimated to be 41% and 80% of that on day 4 after inoculation. These results suggest that neutrophil recruitment at early stages of skin infection was less robust than that on days 2 and 4. Gram staining shows numerous free bacteria inside infection sites on day 1 after inoculation (data not shown). Figure 5D and F show parts of infection sites (at days 2 and 4 after Gram staining) that correspond to the boxed areas in Fig. 5C and E. Parts of infection sites are shown because higher magnification has to be used to show stained GAS bacteria. Stained GAS bacteria were present throughout infection sites that were surrounded by the layer of neutrophils with and without intact nuclei. The layer that is indicated by the braces had no stained GAS bacteria. There were many GAS clumps like the ones circled in Fig. 5D and F, and numerous individual GAS bacteria or bacteria in chains are visible after zooming in by 400% (Fig. 5D and F). These histological data are consistent with our previous finding that the numbers of MGAS2221 bacteria at skin infection sites in C57BL/6J mice were similar from day 1 through day 4 (32). Thus, MGAS2221 was not cleared even with strong neutrophil responses at later time points of infection. The insufficient neutrophil recruitment within day 1 and cytotoxic necrosis of recruited neutrophils should reduce the GAS clearance from the skin. However, we cannot conclude from these results that the

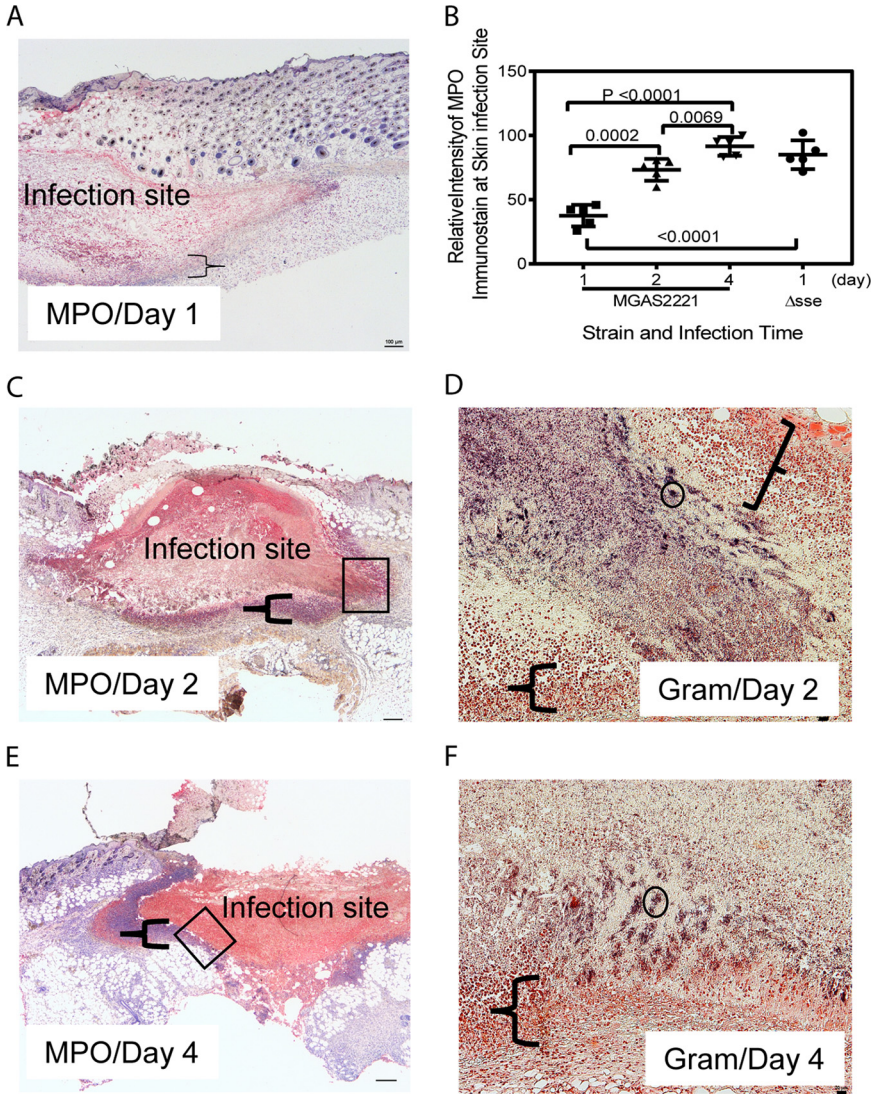

FIG 5 Anti-MPO immunohistochemistry and Gram stainings of subcutaneous MGAS2221 infection sites showing inhibition of neutrophil infiltration, neutrophil necrosis, and GAS persistence. C57BL/6J mice were subcutaneously inoculated with 5.6×10^7 CFU of MGAS2221, and skin containing infection sites were collected at days 1, 2, and 4 after inoculation. Sections of the skin infection sites were stained with anti-MPO antibody and hematoxylin counterstain and examined by IHC. In these MPO IHC/hematoxylin stains, the nucleus (if it was not lost) and MPO in neutrophils were blue and red, respectively. (A, C, and E) Images of MPO IHC/hematoxylin stains for sections of infected lung at days 1 (A), 2 (C), and 4 (E). The braces indicate the layers of neutrophils that surrounded the infection sites and exhibited nuclear staining with hematoxylin. The boxes in panels C and E indicate the locations of the infection sites shown in the Gram stain images in panels D and F, respectively. (B) Relative blue-channel intensities of MPO IHC staining at skin infection sites as estimates of relative levels of recruited neutrophils. The data points are differences in the average intensities of whole infection sites between uninfected and infected mice (5 mice per group). The panels also contain the MPO IHC intensities of MGAS2221 Δ*sse* infection described for Fig. 7. (D and F) Images of Gram staining of the lung sections showing parts of the infection sites located at the places indicated by the boxes in panels C and E. The braces in panels D and F indicate the layers of neutrophils that had intact nuclei, lacked stained GAS bacteria, and surrounded the GAS sites. The circle indicates one of many stained GAS clumps, and numerous GAS organisms as individual bacteria or in chains can be seen after zooming in by 400%. The rest of the infection sites that are not shown exhibited stained GAS. Scale bars: 100 μm (A, C, and E) and 20 μm (D and F).

necrosis of neutrophils critically contributes to the resistance of GAS to clearance from the skin.

Streptolysin S (SLS) has been shown to eradicate neutrophils by inducing nonapoptotic cell death and accelerating apoptosis (37). It is possible that SLS of GAS caused the necrosis of neutrophils at the skin infection site to compromise GAS clearance from

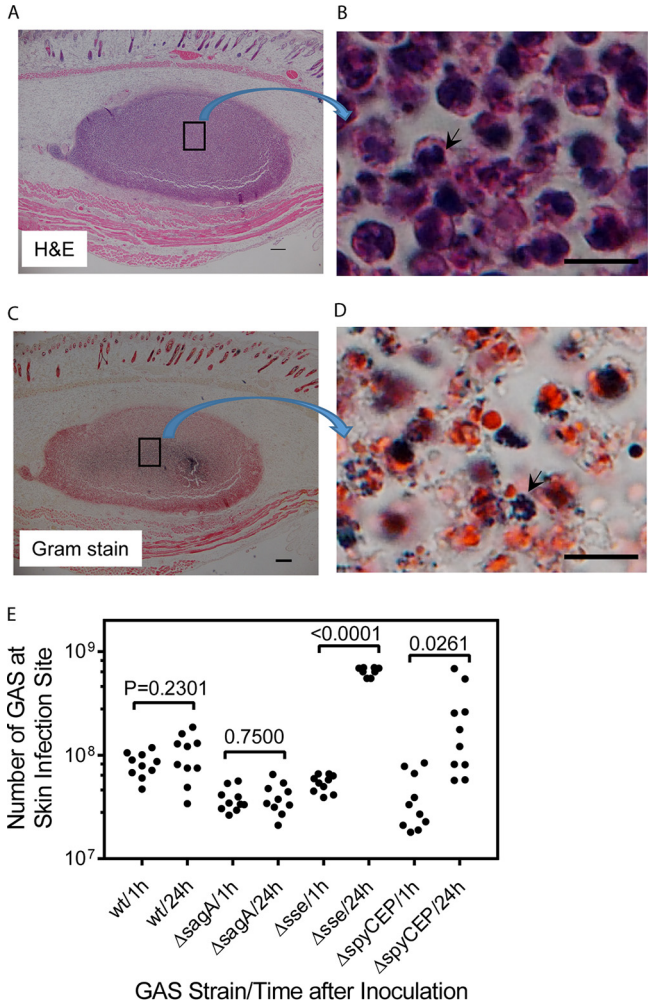

FIG 6 MGAS2221 Δ*sagA* induces robust neutrophil recruitment but is not significantly cleared at skin infection sites of C56BL/6J mice. (A) Representative H&E staining image of a whole Δ*sagA* mutant infection site 24 h after inoculation of 4.1×10^7 CFU of MGAS2221 Δ*sagA* that was full of neutrophils with purple stain. The boxed area in panel A is shown in panel B at higher magnification to demonstrate the blue nuclear staining of neutrophils with hematoxylin. (C) Representative Gram stain image of the whole Δ*sagA* mutant infection site 24 h after inoculation that shows numerous dark-blue spots. The box in panel C is enlarged in panel D to show that the dark-blue spots were dark-blue GAS bacterial clumps. (E) Numbers of GAS bacteria at skin infection sites of C57BL/6J mice at 1 h and 24 h after inoculation of MGAS2221 (wt) and its Δ*sagA*, Δ*sse*, and Δ*spyCEP* mutants. Scale bars: 200 μm (A and C) and 10 μm (B and D).

the skin. To test this possibility, we first deleted the *sagA* gene of MGAS2221, which encodes the SLS peptide (30), yielding SLS-deficient MGAS2221 Δ*sagA*. Then, we tested the MGAS2221 Δ*sagA* mutant in a subcutaneous infection model. MGAS2221 Δ*sagA* caused a small lesion in the subcutaneous infection, and the lesion was full of inflammatory cells that were primarily neutrophils and whose nuclei stained with hematoxylin (Fig. 6A and B). These results indicate that most of the recruited neutrophils had not gone through necrosis at day 1 after MGAS2221 Δ*sagA* inoculation. The Gram stain image of sections of the Δ*sagA* infection sites had numerous dark-blue spots (Fig. 6C), and these dark-blue spots at higher magnification were found to be clumps of bacteria (Fig. 6D). These clumps of bacteria were always colocalized with neutrophils that were stained red with Gram stain but were not present in places without neutrophils. GAS bacteria were apparently associated with neutrophils at Δ*sagA* infection sites. Consistently with the Gram stain results, numbers of MGAS2221 Δ*sagA* bacteria at 24 h after inoculation were 1.04-fold the numbers at 1 h after inoculation (Fig. 6E). Thus, the

robust neutrophil response and elimination of cytotoxic streptolysin S did not lead to MGAS2221 Δ*sagA* clearance from the skin. These results indicate that neutrophils, even without necrosis, cannot effectively clear the MGAS2221 Δ*sagA* mutant from the skin.

Deletion of the *sse* and *spyCEP* genes promotes MGAS2221 proliferation at skin infection sites. The *sse* gene encodes a PAF acetylhydrolase and plays a critical role in inhibition of neutrophil recruitment by hypervirulent M1 and M3 CovRS mutants (26, 39, 40). Anti-MPO staining demonstrated that Δ*sse* mutant infection sites were full of neutrophils (Fig. 7A). Deletion of the *sse* gene enhanced MPO immunostaining at skin infection sites at day 1 by 114% in comparison with that at wt MGAS2221 infection sites at day 1 (Fig. 5B), indicating that the *sse* deletion in MGAS2221 enhanced neutrophil recruitment during skin infection. However, the average number of bacteria at the skin infection sites increased by 11.9-fold, from $(5.4 \pm 1.0) \times 10^7$ CFU at 1 h to $(6.4 \pm 0.6) \times 10^8$ CFU at 24 h postinoculation (Fig. 6E). There was significant growth of the Δ*sse* mutant at skin infection sites. Like the MPO-IHC/hematoxylin staining of MGAS2221 infection sites in C57BL/6 mice in Fig. 5A, neutrophils at the edge of Δ*sse* mutant infection sites exhibited nuclear staining with hematoxylin, which is indicated by the brace, but neutrophils inside Δ*sse* mutant infection sites did not exhibit nuclear staining with hematoxylin in both MPO-IHC/hematoxylin (Fig. 7A) and H&E (Fig. 7B) stainings. Thus, recruited neutrophils inside Δ*sse* mutant infection sites had gone through necrosis. Gram staining shows that there were numerous GAS bacteria throughout Δ*sse* mutant infection sites (Fig. 7C). The *spyCEP* genes encode the peptidase of CXC chemokines, including interleukin-8, and SpyCEP is also involved in the inhibition of neutrophil recruitment (25). Deletion of the *spyCEP* gene also increased GAS numbers at the skin infection sites by 5.7-fold from 1 h to 24 h after inoculation. These results suggest that enhanced neutrophil recruitment at skin infection sites may benefit GAS for growth in the skin.

The phagocyte NADPH oxidase is not required for selection of MGAS2221 SpeB^{A-} variants. GAS with functional CovRS and RopB secretes large quantities of the protease SpeB in Todd-Hewitt broth supplemented with 0.2% yeast extract (THY) at stationary growth phase. The SpeB activity to hydrolyze casein is not detected in the supernatants of stationary cultures of GAS CovRS mutants (41). This phenotype of GAS CovRS mutants is referred as the SpeB activity-negative (SpeB^{A-}) phenotype. SpeB^{A-} variants of MGAS2221 are readily selected during skin infection of mice and account for about 40% of GAS bacteria recovered from infection sites on day 4 after MGAS2221 inoculation (32). Neutrophils play a critical role in the *in vivo* selection of MGAS2221 SpeB^{A-} variants (32). To determine whether the phagocyte NADPH oxidase plays a role in the selection of MGAS2221 SpeB^{A-} variants in skin infection, GAS isolates were recovered from skin infection sites at day 4 after subcutaneous inoculation of MGAS2221 in C57BL/6J and gp91$^{phox-/-}$ mice, and percentages of SpeB^{A-} variants among the recovered isolates from C57BL/6J and gp91$^{phox-/-}$ mice were determined to be 35% and 34%, respectively ($P = 0.8471$) (Fig. 8). Thus, the phagocyte NADPH oxidase is not involved in the selection of SpeB^{A-} variants. This result further supports an insignificant role of the NADPH oxidase in MGAS2221 killing in skin infection, suggesting that GAS can be killed in the skin by NADPH oxidase-independent mechanisms. The numbers of viable GAS bacteria at skin sites were the net results of growth minus killing. Because the numbers of GAS bacteria at MGAS2221 infection sites remain about the same with time, the accumulation of MGAS2221 SpeB^{A-} variants at skin infection sites indicates that there was killing of MGAS2221 at skin infection sites, even though the killing was not sufficient to lead to clearance.

DISCUSSION

This study compared the levels of effectiveness of neutrophils in the clearance of wt M1T1 GAS from the lung and from skin using mouse models of pulmonary and subcutaneous infections to understand the basis for GAS tissue tropism. We report the following major findings: MGAS2221 is effectively cleared from the lung by neutrophils using an NADPH oxidase-dependent mechanism, and neutrophils cannot effectively

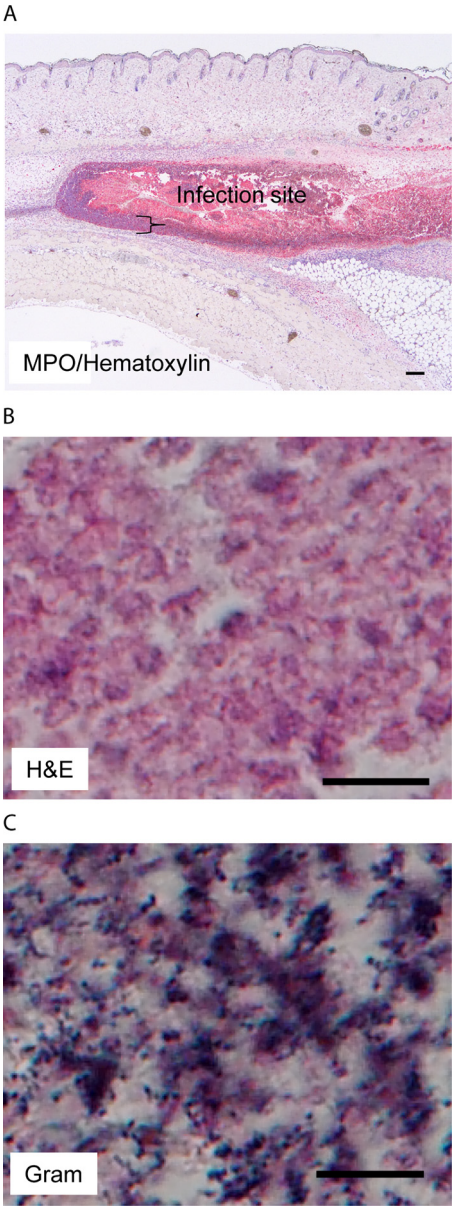

FIG 7 MGAS2221 Δ*sse* skin infection sites are full of necrotic neutrophils that are associated with extensive GAS stains. C57BL/6J mice were subcutaneously inoculated with 5.4×10^7 CFU MGAS2221 Δ*sse*, and skin infection sites were collected at 24 h after inoculation and subjected to histological analyses. (A) Representative MPO IHC/hematoxylin staining image that shows that the Δ*sse* mutant infection site was full of necrotic neutrophils. The brace indicates the layer of neutrophils with nuclear staining with hematoxylin at the edge of the infection site. The MPO staining intensities from the ImageJ analysis are presented in Fig. 5B. (B) Representative H&E staining image for the inside Δ*sse* mutant infection site that shows the lack of nuclear staining with hematoxylin. (C) Representative Gram staining image that shows numerous GAS bacteria with dark-blue stain inside the infection site. The rest of the infection site that is not shown also had numerous stained GAS bacteria. Scale bars: 200 μm (A) and 10 μm (B and C).

clear MGAS2221 and its Δ*sagA*, Δ*spyCEP*, and Δ*sse* mutants in the subcutis. We conclude that wt M1T1 GAS can be sensitive or resistant to clearance by neutrophils depending on whether phagocytic NADPH oxidase-mediated killing is effective or not. The findings are significant in understanding the tissue tropism of GAS.

Intratracheally inoculated wild-type M1T1 GAS bacteria scattered around the bronchial termini, where massive inflammatory cells were recruited, and GAS bacteria were largely cleared by 24 h after inoculation. The recruited inflammatory cells were primarily

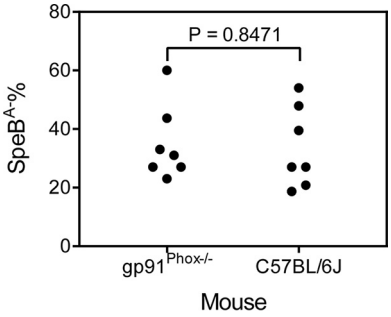

FIG 8 Selection of MGAS2221 SpeB^{A-} variants in C57BL/6J and gp91^{phox} KO mice. Shown are percentages of SpeB^{A-} cells among GAS bacteria recovered from skin infection sites of mice at day 4 after subcutaneous inoculation with 4.4×10^7 CFU of MGAS2221.

neutrophils in C57BL/6 mice. GAS was not cleared from neutropenic mice, and macrophages in BALF from mice with lung infections did not take up M1T1 GAS efficiently. These findings indicate that wt M1T1 GAS is effectively cleared by neutrophils in the lung in the murine intratracheal pneumonia infection model.

Another novel finding is that the skin is a niche where neutrophils are incompetent in the clearance of wt M1T1 GAS. Hypervirulent M1T1 and M3 GAS CovRS mutants inhibit neutrophil infiltration into skin infections, mainly through the function of streptolysin S and the platelet-activating factor (PAF) acetylhydrolase (26, 39–41). MGAS2221 induces robust neutrophil infiltration to the edge of skin infection sites but not inside infection sites at 24 h after inoculation. The inhibition of neutrophil infiltration likely contributes to the resistance of wt M1T1 GAS to clearance at early stages of skin infection but not at later infection stages, since the neutrophil response is present throughout infection sites at days 2 and 4 after inoculation. In contrast, MGAS2221 is persistent at least up to 4 days after inoculation (32). Neutrophils at MGAS2221 infection sites exhibited no nuclear staining with hematoxylin (Fig. 5), indicating that neutrophils were necrotic at these sites. Streptolysin S and the PAF acetylhydrolase play a critical role in the inhibition of neutrophil infiltration and the loss of the nuclear staining during skin infection with a hypervirulent M3 GAS CovS mutant (40). Indeed, skin infection sites with MGAS2221 Δ*sagA* are full of neutrophils with nuclear staining (Fig. 6), demonstrating a critical role of streptolysin S in neutrophil necrosis in wt M1T1 GAS skin infection. Furthermore, streptolysin S reduces or inhibits GAS killing by neutrophils in the intraperitoneal cavities of mice (37). The cytotoxicity of streptolysin S to neutrophils likely contributes to the incompetence of neutrophils to kill GAS in the skin. However, MGAS2221 Δ*sagA* is not effectively cleared from the skin, even though infection sites are full of neutrophils that have intact nuclei. Thus, streptolysin S is not essential for GAS resistance to neutrophil killing during skin infection. These results indicate that the environment in the skin plays a critical role in M1T1 GAS resistance to neutrophil killing. It should be pointed out that we used the subcutaneous infection model for the skin infection. The subcutaneous infection model more closely resembles human necrotizing fasciitis than impetigo or cellulitis skin infections. The histopathological feature described in Fig. 5 is similar to the histopathological feature of the impetigo, the layer of more intense inflammatory cells surrounding infection sites (42). It is most likely that the inefficiency of neutrophils to clear GAS in subcutaneous infections is applicable to GAS-caused impetigo or cellulitis infections.

To cause infection in a particular niche, a pathogen has to be able to survive against immune responses in that niche. The effectiveness and incompetence of neutrophils in GAS clearance from the lung and skin, respectively, are apparently critical factors for the tissue tropism of GAS infections. GAS is the most common bacterial cause of acute pharyngitis, causing approximately 3 and 616 million cases of strep throat annually in the United States and in the world, respectively (1, 43). In contrast, there are about 1,500 cases of pneumonia that are caused by GAS annually in the United States (2).

Thus, GAS infections of the upper respiratory tract rarely lead to infections of the lower respiratory tract. There are 111 million cases of GAS skin infections each year in the world and about 700 cases of necrotizing fasciitis each year in the United States (1, 2). Common GAS skin infections rarely progress into necrotizing fasciitis. Rare necrotizing fasciitis infections are commonly associated with diabetes mellitus on the host side (44), and severe invasive infections are frequently associated with mutations of the virulence regulators CovRS and RopB on the pathogen side (8, 9). The upper respiratory tract and skin are the favorite niches for GAS to cause infections in healthy people. The throat and skin tropisms of GAS have correlations with *emm* types and surface adhesins (19). However, why the skin and throat, but not lung, are the favorite infection sites in healthy people is not well understood. wt M1T1 GAS is effectively cleared from the lung but cannot be effectively cleared by neutrophils from the skin, indicating that neutrophil effectiveness in GAS clearance is correlated with GAS tropism. This notion is further supported by the pathogenesis of hypervirulent GAS mutants. GAS produces an abundance of extracellular virulence factors to mediate pathogenesis, including the M protein, C5a peptidase ScpA, the hyaluronic acid capsule, CXC chemokine peptidase SpyCEP, PAF acetylhydrolase Sse, streptolysin O (Slo), NADase Nga, and the opsonophagocytosis-inhibiting protein Mac. Most of these virulence factors are involved in evasion of neutrophil responses. Natural mutations of CovRS and RopB enhance expression of these virulence genes and evasion of neutrophil responses, enabling GAS infections in the lungs of nonhuman primates and mouse infection models (15, 45).

wt M1T1 GAS is not effectively cleared from the lungs of gp91^{phox} KO mice (Fig. 4). An M23 GAS strain had significantly higher numbers of CFU in blood from p47$^{phox-/-}$ mice than from control mice in an intravascular infection model (46). These findings indicate that NADPH oxidase-dependent killing is a critical mechanism for GAS clearance. The neutrophil NADPH oxidase reduces oxygen to generate superoxide, which dismutes to form H_2O_2. Myeloperoxidase catalyzes the oxidation of Cl^- by H_2O_2 to form bactericidal hypochlorous acid (HOCl). M1T1 GAS is still effectively cleared from the lungs of MPO$^{-/-}$ mice, suggesting that myeloperoxidase is not essential for NADPH oxidase-dependent GAS clearance. However, the GAS clearance data in MPO$^{-/-}$ mice does not rule out the involvement of myeloperoxidase in NADPH oxidase-mediated GAS clearance. It is possible that H_2O_2 generated by the NADPH oxidase-catalyzed reaction kills GAS in MPO$^{-/-}$ mice, since GAS is sensitive to H_2O_2 *in vitro* (47). The lung and blood are oxic environments, which is apparently required for NADPH oxidase-mediated GAS clearance. Hyperbaric oxygen therapy (HBOT) has been used as an adjunctive treatment for streptococcal toxic shock syndrome and necrotizing fasciitis at some medical centers that have HBOT facilities. HBOT for severe GAS infections is controversial but appears to reduce mortality rates (48). NADPH oxidase-mediated killing of GAS by neutrophils is likely the basis for the benefit of HBOT to patients with severe GAS infections.

M1T1 GAS is not effectively cleared at the skin infection site, and there is no significant difference in GAS loads at skin infection sites between gp91^{phox} KO and control mice. These results suggest that NADPH oxidase-mediated killing of GAS is compromised. One possible mechanism for this compromise is that GAS generates an anoxic environment within skin infection sites. GAS causes the occlusion of blood vessels at the skin infection sites by 24 h after GAS inoculation, and blood cannot flow through the infection site (49), which should result in an anoxic environment. GAS does not have catalase, a tricarboxylic acid (TCA) cycle, or oxidative phosphorylation. Therefore, GAS relies completely on the fermentation of sugars for growth and energy production. GAS has lactate oxidase and NADH oxidase (50, 51) and is a facultative anaerobe. An anoxic environment in the skin is thus a favorable niche for allowing anaerobic GAS growth and avoiding NADPH oxidase-mediated killing.

Despite the critical role of the phagocyte NADPH oxidase in GAS clearance from oxic niches, such as the lung and blood, GAS is not associated with chronic granulomatous disease (CGD), which leads to recurrent bacterial infections due to defective phagocyte

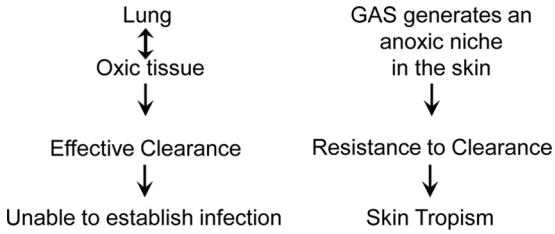

FIG 9 Model of the contribution of the lack of NADPH oxidase-mediated killing to the skin tropism of group A *Streptococcus*. Phagocyte NADPH oxidase-dependent killing plays a critical role in the clearance of GAS. GAS can generate an anoxic niche in the skin to avoid NADPH oxidase-mediated killing, conferring resistance to clearance by neutrophils. In an oxic environment, such as the lung, wt GAS cannot establish infection because of effective NADPH oxidase-mediated killing.

NADPH oxidase activity (52). The most common organisms that cause CGD in patients are catalase-positive bacteria, which are usually part of the normal flora or exist in the environment, such as in soil. In contrast, GAS is a catalase-negative human pathogen. Thus, CGD patients are less susceptible to GAS infections, and GAS thrives better in suboxic and anoxic niches. In the murine intratracheal-pneumonia infection model, hypervirulent GAS CovRS and RopB mutants infected the alveolar region but not the bronchial epithelium (15), indicating that there are additional immune killing mechanisms that prevent GAS infections at certain niches and may also prevent the association of GAS with CGD.

There is a considerable increase in numbers of viable GAS bacteria associated with MGAS2221 Δ*sse* but not MGAS2221 and MGAS2221 Δ*sagA* skin infection sites after inoculation (Fig. 6E). These results indicate that there are NADPH oxidase-independent killing mechanisms of GAS to prevent increases in GAS numbers at skin infection sites, although they are not sufficient to lead to clearance. MGAS2221 SpeB^{A-} variants can be selected by neutrophils at skin infection sites of C57BL/6J mice (32). There was no difference in selection of MGAS2221 SpeB^{A-} variants in C57BL/6J and gp91^{phox} KO mice (Fig. 8), further supporting the existence of NADPH oxidase-independent killing of GAS by neutrophils at skin infection sites. Deletion of the *sse* gene in GAS enhances neutrophil infiltration and reduces skin invasion and systemic dissemination (26, 53). Necrotic neutrophils are associated with extensive staining of GAS bacteria after Gram staining. Apparently, enhanced neutrophil infiltration prevents skin invasion and systemic dissemination but may provide nutrients for MGAS2221 Δ*sse* growth at skin infection sites.

In summary, we have demonstrated that M1T1 GAS is effectively cleared from the lung by neutrophils using an NADPH oxidase-dependent mechanism and that the NADPH oxidase-dependent killing mechanism is compromised in the skin. Thus, our results support a model to explain the skin tropism of GAS. In this model (Fig. 9), phagocyte NADPH oxidase-dependent killing is a critical mechanism for effective clearance of GAS; GAS can generate an anoxic niche in the skin for evading NADPH oxidase-dependent killing by neutrophils and conferring resistance to clearance; in an oxic environment, such as the lung, wt GAS cannot establish infection because of NADPH oxidase-mediated killing.

MATERIALS AND METHODS

Declaration of ethical approval. All animal experimental procedures were carried out in strict accordance with the recommendations in the *Guide for the Care and Use of Laboratory Animals* of the National Institutes of Health (54). The protocols for mouse experiments were approved by the Institutional Animal Care and Use Committee at MSU (protocol numbers 2014-45 and 2017-42).

Bacterial strains and growth. Serotype M1 strain MGAS2221 and its *sagA*, *sse*, and *spyCEP* gene deletion mutants have been described (41, 55). These strains were grown in THY.

Mouse infections. C57BL/6J and gp91^{phox} knockout (female gp91$^{phox-/-}$ and male gp91^{phox-}) mice were bred at the Animal Resource Center at Montana State University (ARC) using breeding pairs of mice from the Jackson Laboratory (Bar Harbor, ME). Myeloperoxidase knockout (MPO KO) mice were purchased from the Jackson Laboratory. To deplete neutrophils in C57BL/6J mice, 250 μg RB6-8C5 (Bio X Cell) in 0.5 ml Dulbecco's phosphate-buffered saline (DPBS) was injected into the intraperitoneal cavity

of each mouse at 24 h prior to GAS inoculation. Control mice were treated similarly with rat IgG2b isotype control monoclonal antibody (MAb) LTF-2. Eight-week-old female (50%) and male (50%) mice were used in pulmonary and skin infections. Because no difference in analyzed data was found between female and male mice, the gender is not indicated for particular data points. GAS bacteria at the exponential growth phase were harvested by centrifugation and washed three times with pyrogen-free DPBS and resuspended in DPBS. Inocula were determined by plating, and the CFU numbers are indicated in the figure legends.

Pulmonary infection was performed, as previously described (15). Mice were anesthetized by 5% isoflurane inhalation and placed in the supine position on an angled platform with the mouth being gently held open. A GAS suspension at an optical density at 600 nm (OD_{600}) of 3 (100 μl) was inoculated through a syringe with a blunt-end needle into the tracheas of mice. At 1 h or 24 h after GAS inoculation, mice were euthanized with a gradual fill method at a displacement rate of 30% CO_2 of the chamber volume per minute, as recommended in the 2013 guidelines of the American Veterinary Medical Association (56). The lung was then lavaged or collected for cytospin and histological analyses or measurements of GAS loads. For skin infection, 0.2 ml of GAS in DPBS at an OD_{600} of 1.0 was inoculated subcutaneously into mice. Mice were then euthanized at 1 h or 24 h after inoculation, and skin infection sites were collected for histological analyses and quantification of viable GAS bacteria.

Quantification of GAS numbers in lung and skin infection sites. Parts of the lungs were collected and weighed for the pulmonary infection, and a piece of skin containing the whole infection site was collected for the skin infection. The lung and skin samples were homogenized in DPBS using a Kontes pestle and plated at appropriate dilutions.

Cytospin analysis. The lungs of euthanized mice were lavaged with 1 ml of DPBS to collect BALF. An aliquot of the recovered lavage fluid was used to determine the total number of viable cells by trypan blue exclusion counting. A second aliquot of the recovered lavage fluid at an appropriate dilution was used to prepare cytospin slides using a Shandon cytospin cytocentrifuge. The slides were stained using the Diff-Quik stain kit from Fisher Scientific. Neutrophils and macrophages among 150 host cells on each cytospin slide were counted to determine the percentages of neutrophils and macrophages, and the total numbers of neutrophils and macrophages were calculated from the percentage data and the total counts of viable cells in the lavage samples. A third aliquot of the BALF samples was plated at an appropriate dilution to count numbers of GAS bacteria.

Histological analyses. The lungs of euthanized mice were perfused with 10% formalin and fixed in 10% formalin for 24 h. Skin samples containing GAS infection sites were also fixed in 10% formalin for 24 h. The fixed samples were dehydrated with ethanol, cleared with xylene, and infiltrated with paraffin using a tissue-embedding console system (Sakura Finetek, Inc.). The paraffin blocks were cut to obtain 4-μm sections, which were stained with hematoxylin and eosin (H&E) or with a Gram stain kit from Becton, Dickinson and Company. For immunostaining, deparaffinized tissue sections were treated in boiling citrate, pH 6.0, for 25 min for antigen retrieval, washed with DPBS, blocked with Biocare rodent block M (item no. RBM961H), and incubated with rabbit anti-myeloperoxidase antibody from Abcam (item no. ab139748) or rat anti-mouse F4/80 antibody from Bio-Rad (item no. MCA497R). The slides were washed with Tris-buffered saline–0.5% Tween 20 (TBS-T), incubated with Biocare's Rabbit-on-Rodent AP-Polymer for myeloperoxidase staining or Rat-on-Mouse AP-Polymer for F4/80 staining, washed with TBS-T, and developed with a Biocare Vulcan Red fast-stain kit. Immunostained slides were mounted with ProLong Gold antifade mountant with DAPI (4′,6-diamidino-2-phenolindole) from Invitrogen. Stained slides were examined using a Nikon Eclipse 80i microscope.

The ImageJ software (https://imagej.nih.gov/ij/) was used to measure the average intensities of MPO IHC staining for the IHC/hematoxylin staining images of subcutaneous infection sites and uninfected skin. Images were first split into images of red, green, and blue channels. The whole infection site of the blue-channel image was selected, and the average intensity was measured. Blue-channel images were used to reduce the interference of hematoxylin staining of some neutrophils. The relative MPO staining intensities are the differences in the average intensities between uninfected and infected samples (the intensities of the uninfected skin minus the intensities of infection sites).

Selection of SpeB^{A-} variants in mice. Analysis of an *in vivo* selection of SpeB^{A-} variants of clinical GAS isolates was performed, as described previously (32). Briefly, female C57BL/6J and gp91^{phox} KO mice were inoculated with 4.4×10^7 CFU of MGAS2221 and euthanized on day 4 after inoculation. Skin infection sites were collected and homogenized in 1.0 ml DPBS using a Kontes pestle. The samples were then plated at appropriate dilutions, and 48 colonies for each mouse were randomly picked, inoculated in 200 μl THY in 96-well plates, and cultured overnight at 37°C in 5% CO_2. Three microliters of 10% β-mercaptoethanol was added into each well, and 15 μl of the supernatant was loaded into wells of casein gel plates and incubated at 37°C for 5 h. The lack of the cloudy ring indicated a lack of SpeB activity in the samples (SpeB^{A-}). The number of SpeB^{A-} colonies among 48 colonies from a mouse was counted to calculate the percentage of SpeB^{A-} variants among GAS bacteria recovered from each mouse.

Statistical analyses. The statistical analyses were performed using the unpaired *t* test with Welch's correction of the GraphPad Prism software (version 7.03).

ACKNOWLEDGMENTS

This work was supported in part by grants AI095704 and GM110732 from the National Institutes of Health and by the Montana State Agricultural Experimental Station.

REFERENCES

1. Carapetis JR, Steer AC, Mulholland EK, Weber M. 2005. The global burden of group A streptococcal diseases. Lancet Infect Dis 5:685–694. https://doi.org/10.1016/S1473-3099(05)70267-X.
2. Nelson GE, Pondo T, Toews KA, Farley MM, Lindegren ML, Lynfield R, Aragon D, Zansky SM, Watt JP, Cieslak PR, Angeles K, Harrison LH, Petit S, Beall B, Van Beneden CA. 2016. Epidemiology of invasive group A streptococcal infections in the United States, 2005–2012. Clin Infect Dis 63:478–486. https://doi.org/10.1093/cid/ciw248.
3. Sumby P, Porcella SF, Madrigal AG, Barbian KD, Virtaneva K, Ricklefs SM, Sturdevant DE, Graham MR, Vuopio-Varkila J, Hoe NP, Musser JM. 2005. Evolutionary origin and emergence of a highly successful clone of serotype M1 group a Streptococcus involved multiple horizontal gene transfer events. J Infect Dis 192:771–782. https://doi.org/10.1086/432514.
4. Maamary PG, Ben Zakour NL, Cole JN, Hollands A, Aziz RK, Barnett TC, Cork AJ, Henningham A, Sanderson-Smith M, McArthur JD, Venturini C, Gillen CM, Kirk JK, Johnson DR, Taylor WL, Kaplan EL, Kotb M, Nizet V, Beatson SA, Walker MJ. 2012. Tracing the evolutionary history of the pandemic group A streptococcal M1T1 clone. FASEB J 26:4675–4684. https://doi.org/10.1096/fj.12-212142.
5. Nasser W, Beres SB, Olsen RJ, Dean MA, Rice KA, Long SW, Kristinsson KG, Gottfredsson M, Vuopio J, Raisanen K, Caugant DA, Steinbakk M, Low DE, McGeer A, Darenberg J, Henriques-Normark B, Van Beneden CA, Hoffmann S, Musser JM. 2014. Evolutionary pathway to increased virulence and epidemic group A *Streptococcus* disease derived from 3,615 genome sequences. Proc Natl Acad Sci U S A 111:E1768–1776. https://doi.org/10.1073/pnas.1403138111.
6. Colman G, Tanna A, Efstratiou A, Gaworzewska ET. 1993. The serotypes of Streptococcus pyogenes present in Britain during 1980–1990 and their association with disease. J Med Microbiol 39:165–178. https://doi.org/10.1099/00222615-39-3-165.
7. Feng W, Liu M, Chen DG, Yiu R, Fang FC, Lei B. 2016. Contemporary pharyngeal and invasive emm1 and invasive emm12 group A Streptococcus isolates exhibit similar in vivo selection for CovRS mutants in mice. PLoS One 11:e0162742. https://doi.org/10.1371/journal.pone.0162742.
8. Ikebe T, Ato M, Matsumura T, Hasegawa H, Sata T, Kobayashi K, Watanabe H. 2010. Highly frequent mutations in negative regulators of multiple virulence genes in group A streptococcal toxic shock syndrome isolates. PLoS Pathog 6:e1000832. https://doi.org/10.1371/journal.ppat.1000832.
9. Shea PR, Beres SB, Flores AR, Ewbank AL, Gonzalez-Lugo JH, Martagon-Rosado AJ, Martinez-Gutierrez JC, Rehman HA, Serrano-Gonzalez M, Fittipaldi N, Ayers SD, Webb P, Willey BM, Low DE, Musser JM. 2011. Distinct signatures of diversifying selection revealed by genome analysis of respiratory tract and invasive bacterial populations. Proc Natl Acad Sci U S A 108:5039–5044. https://doi.org/10.1073/pnas.1016282108.
10. Levin JC, Wessels MR. 1998. Identification of csrR/csrS, a genetic locus that regulates hyaluronic acid capsule synthesis in group A Streptococcus. Mol Microbiol 30:209–219. https://doi.org/10.1046/j.1365-2958.1998.01057.x.
11. Heath A, DiRita VJ, Barg NL, Engleberg NC. 1999. A two-component regulatory system, CsrR-CsrS, represses expression of three *Streptococcus pyogenes* virulence factors, hyaluronic acid capsule, streptolysin S, and pyrogenic exotoxin B. Infect Immun 67:5298–5305.
12. Federle MJ, McIver KS, Scott JR. 1999. A response regulator that represses transcription of several virulence operons in the group A *Streptococcus*. J Bacteriol 181:3649–3657.
13. Treviño J, Perez N, Ramirez-Peña E, Liu Z, Shelburne SA, Musser JM, Sumby P. 2009. CovS simultaneously activates and inhibits the CovR-mediated repression of distinct subsets of group A Streptococcus virulence factor-encoding genes. Infect Immun 77:3141–3149. https://doi.org/10.1128/IAI.01560-08.
14. Dmitriev AV, McDowell EJ, Chaussee MS. 2008. Inter- and intraserotypic variation in the *Streptococcus pyogenes* Rgg regulon. FEMS Microbiol Lett 284:43–51. https://doi.org/10.1111/j.1574-6968.2008.01171.x.
15. Lei B, Minor D, Feng W, Liu M. 2018. Hypervirulent group A Streptococcus of genotype *emm3* invades the vascular system in pulmonary infection of mice. Infect Immun 86:e00080-18. https://doi.org/10.1128/IAI.00080-18.
16. Olsen RJ, Raghuram A, Cantu C, Hartman MH, Jimenez FE, Lee S, Ngo A, Rice KA, Saddington D, Spillman H, Valson C, Flores AR, Beres SB, Long SW, Nasser W, Musser JM. 2015. The majority of 9,729 group A streptococcus strains causing disease secrete SpeB cysteine protease: pathogenesis implications. Infect Immun 83:4750–4758. https://doi.org/10.1128/IAI.00989-15.
17. Lancefield RC. 1962. Current knowledge of type-specific M antigens of group A streptococci. J Immunol 89:307–313.
18. Beall B, Facklam R, Thompson T. 1996. Sequencing emm-specific PCR products for routine and accurate typing of group A streptococci. J Clin Microbiol 34:953–958.
19. Bessen DE. 2016. Tissue tropisms in group A Streptococcus: what virulence factors distinguish pharyngitis from impetigo strains? Curr Opin Infect Dis 29:295–303. https://doi.org/10.1097/QCO.0000000000000262.
20. Lei B, Mackie S, Lukomski S, Musser JM. 2000. Identification and immunogenicity of group A *Streptococcus* culture supernatant proteins. Infect Immun 68:6807–6818. https://doi.org/10.1128/iai.68.12.6807-6818.2000.
21. Cunningham MW. 2000. Pathogenesis of group A streptococcal infections. Clin Microbiol Rev 13:470–511. https://doi.org/10.1128/cmr.13.3.470-511.2000.
22. Fischetti VA. 1989. Streptococcal M protein: molecular design and biological behavior. Clin Microbiol Rev 2:285–314. https://doi.org/10.1128/cmr.2.3.285.
23. Cleary P, Prabu U, Dale J, Wexler D, Handley J. 1992. Streptococcal C5a peptidase is a highly specific endopeptidase. Infect Immun 60:5219–5223.
24. Wessels MR, Goldberg JB, Moses AE, DiCesare TJ. 1994. Effects on virulence of mutations in a locus essential for hyaluronic acid capsule expression in group A streptococci. Infect Immun 62:433–441.
25. Edwards RJ, Taylor GW, Ferguson M, Murray S, Rendell N, Wrigley A, Bai Z, Boyle J, Finney SJ, Jones A, Russell HH, Turner C, Cohen J, Faulkner L, Sriskandan S. 2005. Specific C-terminal cleavage and inactivation of interleukin-8 by invasive disease isolates of *Streptococcus pyogenes*. J Infect Dis 192:783–790. https://doi.org/10.1086/432485.
26. Liu M, Zhu H, Li J, Garcia CC, Feng W, Kirpotina LN, Hilmer J, Tavares LP, Layton AW, Quinn MT, Bothner B, Teixeira MM, Lei B. 2012. Group A *Streptococcus* secreted esterase hydrolyzes platelet-activating factor to impede neutrophil recruitment and facilitate innate immune evasion. PLoS Pathog 8:e1002624. https://doi.org/10.1371/journal.ppat.1002624.
27. O'Seaghdha M, Wessels MR. 2013. Streptolysin O and its co-toxin NAD-glycohydrolase protect group A *Streptococcus* from xenophagic killing. PLoS Pathog 9:e1003394. https://doi.org/10.1371/journal.ppat.1003394.
28. Bricker AL, Carey VJ, Wessels MR. 2005. Role of NADase in virulence in experimental invasive group A streptococcal infection. Infect Immun 73:6562–6566. https://doi.org/10.1128/IAI.73.10.6562-6566.2005.
29. Lei B, DeLeo FR, Hoe NP, Graham MR, Mackie SM, Cole RL, Liu M, Hill HR, Low DE, Federle MJ, Scott JR, Musser JM. 2001. Evasion of human innate and acquired immunity by a bacterial homolog of CD11b that inhibits opsonophagocytosis. Nat Med 7:1298–1305. https://doi.org/10.1038/nm1201-1298.
30. Nizet V, Beall B, Bast DJ, Datta V, Kilburn L, Low DE, De Azavedo JC. 2000. Genetic locus for streptolysin S production by group A streptococcus. Infect Immun 68:4245–4254. https://doi.org/10.1128/iai.68.7.4245-4254.2000.
31. Daley JM, Thomay AA, Connolly MD, Reichner JS, Albina JE. 2008. Use of Ly6G-specific monoclonal antibody to deplete neutrophils in mice. J Leukoc Biol 83:64–70. https://doi.org/10.1189/jlb.0407247.
32. Li J, Liu G, Feng W, Zhou Y, Liu M, Wiley JA, Lei B. 2014. Neutrophils select hypervirulent CovRS mutants of M1T1 group A Streptococcus during subcutaneous infection of mice. Infect Immun 82:1579–1590. https://doi.org/10.1128/IAI.01458-13.
33. Bainton DF, Ullyot JL, Farquhar MG. 1971. The development of neutrophilic polymorphonuclear leukocytes in human bone marrow. J Exp Med 134:907. https://doi.org/10.1084/jem.134.4.907.
34. Hampton MB, Kettle AJ, Winterbourn CC. 1998. Inside the neutrophil phagosome: oxidants, myeloperoxidase, and bacterial killing. Blood 92:3007–3017.
35. Pollock JD, Williams DA, Gifford MA, Li LL, Du X, Fisherman J, Orkin SH, Doerschuk CM, Dinauer MC. 1995. Mouse model of X-linked chronic granulomatous disease, an inherited defect in phagocyte superoxide production. Nat Genet 9:202–209. https://doi.org/10.1038/ng0295-202.
36. Brennan ML, Anderson MM, Shih DM, Qu XD, Wang X, Mehta AC, Lim LL,

Shi W, Hazen SL, Jacob JS, Crowley JR, Heinecke JW, Lusis AJ. 2001. Increased atherosclerosis in myeloperoxidase-deficient mice. J Clin Invest 107:419–430. https://doi.org/10.1172/JCI8797.
37. Miyoshi-Akiyama T, Takamatsu D, Koyanagi M, Zhao J, Imanishi K, Uchiyama T. 2005. Cytocidal effect of Streptococcus pyogenes on mouse neutrophils in vivo and the critical role of streptolysin S. J Infect Dis 192:107–116. https://doi.org/10.1086/430617.
38. Wikipedia contributors. 13 July 2016. Necrosis, on Wikipedia, The Free Encyclopedia. https://librepathology.org/wiki/Necrosis. Accessed 8 July 2019.
39. Stetzner ZW, Li D, Feng W, Liu M, Liu G, Wiley J, Lei B. 2015. Serotype M3 and M28 group A streptococci have distinct capacities to evade neutrophil and TNF-α responses and to invade soft tissues. PLoS One 10: e0129417. https://doi.org/10.1371/journal.pone.0129417.
40. Feng W, Minor D, Liu M, Lei B. 2017. Requirement and synergistic contribution of platelet-activating factor acetylhydrolase Sse and streptolysin S to inhibition of neutrophil recruitment and systemic infection by hypervirulent *emm3* group A Streptococcus in subcutaneous infection of mice. Infect Immun 85:e00530-17. https://doi.org/10.1128/IAI.00530-17.
41. Li J, Zhu H, Feng W, Liu M, Song Y, Zhang X, Zhou Y, Bei W, Lei B. 2013. Regulation of inhibition of neutrophil infiltration by the two-component regulatory system CovRS in subcutaneous murine infection with group A streptococcus. Infect Immun 81:974–983. https://doi.org/10.1128/IAI.01218-12.
42. Plaza JA, Frieto VG. 2009. Inflammatory skin conditions. Mod Surg Pathol 2:1843–1889.
43. Bisno AL. 1996. Acute pharyngitis: etiology and diagnosis. Pediatrics 97:949–954.
44. Wong CH, Chang HC, Pasupathy S, Khin LW, Tan JL, Low CO. 2003. Necrotizing fasciitis: clinical presentation, microbiology, and determinants of mortality. J Bone Joint Surg Am 85-A:1454–1460. https://doi.org/10.2106/00004623-200308000-00005.
45. Olsen RJ, Ashraf M, Gonulal VE, Ayeras AA, Cantu C, Shea PR, Carroll RK, Humbird T, Greaver JL, Swain JL, Chang E, Ragasa W, Jenkins L, Lally KP, Blasdel T, Cagle P, Musser JM. 2010. Lower respiratory tract infection in cynomolgus macaques (Macaca fascicularis) infected with group A Streptococcus. Microb Pathog 49:336–347. https://doi.org/10.1016/j.micpath.2010.06.012.
46. Goldmann O, von Köckritz-Blickwede M, Höltje C, Chhatwal GS, Geffers R, Medina E. 2007. Transcriptome analysis of murine macrophages in response to infection with Streptococcus pyogenes reveals an unusual activation program. Infect Immun 75:4148–4157. https://doi.org/10.1128/IAI.00181-07.
47. Ricci S, Janulczyk R, Björck L. 2002. The regulator PerR is involved in oxidative stress response and iron homeostasis and is necessary for full virulence of Streptococcus pyogenes. Infect Immun 70:4968–4976. https://doi.org/10.1128/iai.70.9.4968-4976.2002.
48. Shaw JJ, Psoinos C, Emhoff TA, Shah SA, Santry HP. 2014. Not just full of hot air: hyperbaric oxygen therapy increases survival in cases of necrotizing soft tissue infections. Surg Infect (Larchmt) 15:328–335. https://doi.org/10.1089/sur.2012.135.
49. Liu M, Feng W, Zhu H, Lei B. 2015. A neutralizing monoclonal IgG1 antibody of platelet-activating factor acetylhydrolase SsE protects mice against lethal subcutaneous group A Streptococcus infection. Infect Immun 83:2796–2805. https://doi.org/10.1128/IAI.00073-15.
50. Gibson CM, Mallett TC, Claiborne A, Caparon MG. 2000. Contribution of NADH oxidase to aerobic metabolism of Streptococcus pyogenes. J Bacteriol 182:448–455. https://doi.org/10.1128/jb.182.2.448-455.2000.
51. Seki M, Iida K, Saito M, Nakayama H, Yoshida S. 2004. Hydrogen peroxide production in Streptococcus pyogenes: involvement of lactate oxidase and coupling with aerobic utilization of lactate. J Bacteriol 186: 2046–2051. https://doi.org/10.1128/jb.186.7.2046-2051.2004.
52. Heyworth P, Cross A, Curnutte J. 2003. Chronic granulomatous disease. Curr Opin Immunol 15:578–784. https://doi.org/10.1016/S0952-7915(03)00109-2.
53. Zhu H, Liu M, Sumby P, Lei B. 2009. The secreted esterase of group a streptococcus is important for invasive skin infection and dissemination in mice. Infect Immun 77:5225–5232. https://doi.org/10.1128/IAI.00636-09.
54. National Research Council. 2011. Guide for the care and use of laboratory animals, 8th ed. National Academies Press, Washington, DC.
55. Zhou Y, Hanks TS, Feng W, Li J, Liu G, Liu M, Lei B. 2013. The sagA/pel locus does not regulate the expression of the M protein of the M1T1 lineage of group A Streptococcus. Virulence 4:698–706. https://doi.org/10.4161/viru.26413.
56. American Veterinary Medical Association. 2013. AVMA guidelines for the euthanasia of animals: 2013 edition. AVMA, Schaumburg, IL. https://www.avma.org/KB/Policies/Documents/euthanasia.pdf.